

Banner appropriate to article type will appear here in typeset article

Towards decoupling the effects of permeability and roughness on turbulent boundary layers

D. D. Wangsawijaya¹†, P. Jaiswal^{1,2} and B. Ganapathisubramani¹

¹Aeronautical and Astronautical Engineering, University of Southampton SO17 1BJ, United Kingdom

²Department of Mechanical Engineering, University of Sherbrooke, Sherbrooke, QC, J1K 2R1, Canada

(Received xx; revised xx; accepted xx)

Boundary layer flow over a realistic porous wall might contain both the effects of wall-permeability and wall-roughness. These two effects are typically examined in the context of a rough-wall flow, i.e., by defining a “roughness” length or equivalent to capture the effect of the surface on momentum deficit/drag. In this work, we examine the hypothesis of Esteban *et al.* (2022), that a turbulent boundary layer over a porous wall could be modelled as a superposition of the roughness effects on the permeability effects by using independently obtained information on permeability and roughness. We carry out wind tunnel experiments at high Reynolds number ($14400 \leq Re_\tau \leq 33100$) on various combinations of porous walls where different roughnesses are overlaid over a given permeable wall. Measurements are also conducted on the permeable wall as well as the rough walls independently to obtain the corresponding lengthscales. Analysis of mean flow data across all these measurements suggests that an empirical formulation can be obtained where the momentum deficit (ΔU^+) is modelled as a combination of independently obtained roughness and permeability lengthscales. This formulation assumes the presence of outer-layer similarity across these different surfaces, which is shown to be valid at high Reynolds numbers. Finally, this decoupling approach is equivalent to the area-weighted power-mean of the respective permeability and roughness lengthscales, consistent with the approach recently suggested by Hutchins *et al.* (2023) to capture the effects of heterogeneous rough surfaces.

Key words:

1. Introduction

Flow over porous walls comprises an extensive number of natural phenomena, ranging from blood vessels to the atmospheric boundary layer (ABL) developing over a forest canopy. The latter can be considered as a turbulent boundary layer (TBL) developing over a porous wall. An example of porous walls, constructed from packed spheres, is shown in figure 1. Here, both walls approximately have the same permeability (resistance of a substrate to fluid flows), but the wall shown in figure 1(a) has a roughness interface above the porous wall,

† Email address for correspondence: D.D.Wangsawijaya@soton.ac.uk

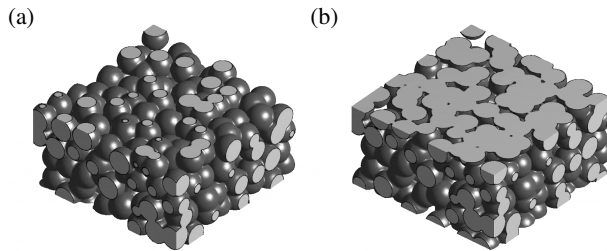


Figure 1: Illustrations of realistic permeable walls with: (a) a rough wall on the interface and (b) flat interface. Adapted from Rosti *et al.* (2015).

while in figure 1(b) this interface comprises of a flat surface. Thus, a realistic representation of a porous wall is *both* permeable *and* rough to some extent; for the wall in figure 1(a), the effects of both permeability and roughness have to be considered for characterisation of a TBL developing over such wall.

1.1. Rough walls

The presence of rough walls increases skin friction from that of smooth walls and thus the time-averaged streamwise velocity U of TBLs developing over rough walls can be written as a downward shift of the logarithmic region ΔU^+ from the smooth wall velocity profile

$$U^+ = \frac{1}{\kappa} \ln \left[\frac{(y+d)U\tau}{\nu} \right] + B - \Delta U^+ = \frac{1}{\kappa} \ln(y+y_0)^+ + B - \Delta U^+ \quad (1.1)$$

The viscous-scaled velocity is defined as $U^+ \equiv U/U_\tau$, where $U_\tau \equiv \sqrt{\tau_w/\rho}$ is the friction velocity, τ_w and ρ are the wall shear stress (WSS) and the density of fluid, respectively. The logarithmic profile is defined as follows: κ is the von Kármán constant, d is the zero-plane displacement, ν is the kinematic viscosity of fluid, and B is the log-law intercept. The logarithmic shift ΔU^+ , also known as the Hama roughness function (Hama 1954), is defined as

$$\Delta U^+ = \frac{1}{\kappa} \ln \left(\frac{k_s U_\tau}{\nu} \right) + B - B_{FR} = \frac{1}{\kappa} \ln k_s^+ + B - B_{FR} \quad (1.2)$$

where k_s is the equivalent sand grain roughness and $B_{FR} = 8.5$ is the ‘fully’ rough intercept of the velocity profile of sand grain roughness. It should be noted that k_s is a measure of roughness effect on the flow relative to that of a uniform sand grain roughness (Nikuradse 1933); it can only be determined by flow measurements. The mean streamwise velocity profile of a rough wall can therefore be written as a function of its k_s

$$U^+ = \frac{1}{\kappa} \ln \left(\frac{y+d}{k_s} \right) + B_{FR} \quad (1.3)$$

1.2. Permeable walls

Earlier studies of TBLs developing over permeable walls involved various types of such walls, namely: packed spheres (Zagni & Smith 1976), perforated sheets (Kong & Schetz 1982), bed of grains (Zippe & Graf 1983), and multi-layered walls (Manes *et al.* 2009). Permeable walls have been found to increase drag (i.e. skin friction coefficient $C_f \equiv 2(U_\tau/U_\infty)^2$) from that of solid, impermeable walls, which is attributed to the increase of dissipation, momentum flux, and Reynolds shear stress on the interface between the fluid and the substrates (Zagni & Smith 1976; Shimizu *et al.* 1990). Similar to the rough wall TBLs, the increase in C_f of permeable walls is also characterised by a downward shift in the logarithmic region from that

of a solid, smooth wall (Hahn *et al.* 2002; Efstathiou & Luhar 2018). Thus, it is probable that there is a “universal” parameter that characterise permeable walls – possibly equivalent to k_s for rough wall TBLs. It was suggested by Manes *et al.* (2011) that the logarithmic region of a TBL developing over a permeable wall scales on permeability K , and this can be further rearranged to show a downward logarithmic shift,

$$U^+ = \frac{1}{\kappa} \ln \left(\frac{y+d}{\sqrt{K}} \right) + c_1 = \frac{1}{\kappa} \ln(y+d)^+ - \frac{1}{\kappa} \ln Re_K + c_1 \quad (1.4)$$

where $Re_K \equiv \sqrt{K}U_\tau/\nu$. Previous studies observed a wide range of magnitude of κ (Breugem *et al.* 2006; Manes *et al.* 2011; Suga *et al.* 2010), which is largely attributed to the low Re at which these studies were conducted and thus there was not enough separation between the inner and outer layers of the wall-bounded flows (Manes *et al.* 2011). A more recent experimental work by Esteban *et al.* (2022), conducted at a higher order of magnitude of Re ($2000 \leq Re_\tau \leq 18000$), observed that $\kappa = 0.39$, similar to that of smooth and rough wall TBLs. It was further hypothesised by Esteban *et al.* (2022) that c_1 in equation (1.4) is an additive constant related to the blockage effect of a porous substrate, as a realistic porous wall comprises of both permeable matrix and solid substrates (see, for example, figure 1), whose size does not permit the full isolation of permeability effect (Breugem *et al.* 2006). This blockage effect might be represented by a roughness function $\Delta U_b^+ \equiv 1/\kappa \ln k_{sb}^+ + B - B_{FR}$, similar to that of equation (1.2)

$$U^+ = \frac{1}{\kappa} \ln(y+d)^+ - \frac{1}{\kappa} \ln Re_K - \frac{1}{\kappa} \ln k_{sb}^+ + B_{FR} = \frac{1}{\kappa} \ln \left(\frac{y+d}{Re_K k_{sb}} \right) + B_{FR} \quad (1.5)$$

where subscript ‘ b ’ denote the blockage effect of the porous substrate. By comparing equation (1.3) and (1.5), the ‘equivalent sand grain roughness’ k_s of a porous wall (subscript ‘ p ’) can be defined as

$$k_{s_p} = Re_K k_{sb} \quad (1.6)$$

In this study, we take the first steps towards exploring the possibility of decoupling permeability and roughness effects on turbulent boundary layers. We have constructed three different porous test surfaces where we maintain the permeability (Re_K) but the blockage is systematically altered by adding roughness on to a given permeable substrate. Detailed hot-wire and drag-balance measurements are taken for the permeable, rough and the combination of permeable-rough surfaces over a wide range of Reynolds numbers (ensuring the flow is in fully-rough regime for all cases). We use the experimental data to explore two different approaches for decoupling the two effects. First, we extend the above-mentioned framework to include the effects of additional roughness. Second, we use a power-mean averaging approach proposed for heterogeneous roughness (Hutchins *et al.* 2023) to find an equivalent roughness lengthscale that can capture the combined effect of permeability and roughness.

2. Experimental Setup

2.1. Facility

Measurements are conducted inside the closed return boundary layer wind tunnel (BLWT) at the University of Southampton. The flow passes through a contraction section of 6:1 ratio before entering the 12 m × 1.2 m × 1 m (length × width × height) test section. The boundary layer develops over the floor (bottom surface) of the BLWT. A 220 mm-long smooth wall ramp is installed at the end of the contraction section (figure 2(a)Ⓐ) to match the thickness of the test surfaces. This ramp marks the inlet towards the test section of the BLWT and

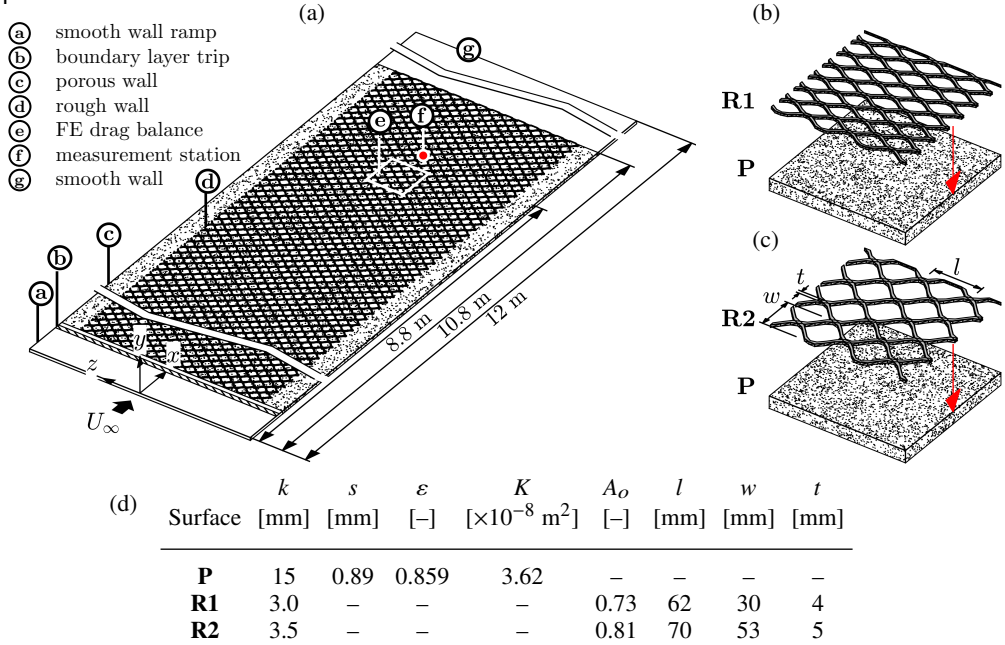


Figure 2: (a) Illustration of a test surface laid inside the test section of the boundary layer wind tunnel. Combination of porous-rough test surfaces: (b) porous **P**-rough wall **R1**, and (c) porous **P**-rough wall **R2**. (d) Geometric parameters of **P**, **R1**, and **R2**, where k is the thickness of the surfaces. For **P**: s is the average pore size of the foam, ε is the porosity, and K is the permeability, obtained from Esteban *et al.* (2022). For **R1** and **R2**: A_o is the open area ratio of the mesh, l is the length of the longway of the mesh, w is the length of the shortway of the mesh, and t is the width of the mesh strand, as illustrated in (c).

the streamwise datum ($x = 0$). The boundary layer is tripped by a 8.5 mm-wide, 0.4 mm-thick turbulator tape attached on the ramp (figure 2(a)(b)). The tunnel has the freestream turbulence level of $\sigma_{u'}/U_\infty \approx 0.1\%$, where $\sigma_{u'}$ is the standard deviation of streamwise turbulent fluctuation at the freestream and U_∞ is the freestream velocity. The BLWT is equipped with a water-cooled heat exchanger, maintaining the flow temperature variation of 1% for the longest measurements (~ 8 hours).

2.2. Test surfaces

Five test surfaces are constructed for this study: porous wall (denoted by ‘**P**’, figure 2(a)(c)), two types of rough walls (‘**R1**’ and ‘**R2**’, figure 2b,c), and two combinations of rough walls on top of the porous wall (‘**PR1**’ and ‘**PR2**’, figure 2b,c). All test surfaces are assembled on the bottom surface of the BLWT, downstream of the ramp and trip (figure 2a). The ramp and test surfaces only cover the first 10.8 m-long part of the test section, while the section from $x = 10.8$ m to $x = 12$ m comprises of a smooth wall (figure 2a). All measurements are conducted at a constant x location at a range freestream velocity U_∞ , corresponding to a set of matched friction Reynolds number $Re_\tau \equiv \delta U_\tau / \nu \pm 1600$ (here, δ is the 99% boundary-layer thickness) between **P**, **R1**, and **PR1**, as well as another set of matched Re_τ for **P**, **R2**, and **PR2**. The first set of test surfaces has 5 matched Re_τ cases ($Re_\tau \approx 14400, 18600, 23400, 22900$, and, 33100), while the second set has four matched cases ($Re_\tau \approx 14400, 18600, 23400$, and 27700). Details of each test surfaces, including the statistics obtained from HWA and WSS measurements, are given in table 1. Throughout this study, each test surface is denoted with a symbol (see the last column in table 1). The same colour denotes surfaces

Case	δ [mm]	θ [mm]	U_∞ [ms ⁻¹]	U_τ [ms ⁻¹]	Re_x [$\times 10^7$]	Re_θ [$\times 10^4$]	Re_τ [$\times 10^4$]	Re_K [-]	C_f [$\times 10^{-3}$]	Π [-]	ΔU^+ [-]	k_s [mm]	k_s^+ [-]	Sym.
Porous walls														
P	201.11	24.55	19.84	1.06	1.18	3.29	1.44	13.62	5.72	0.27	12.01		560	○
	199.96	24.45	25.45	1.36	1.52	4.21	1.85	17.57	5.74	0.27	12.66		723	○
	208.26	25.37	29.06	1.54	1.76	5.07	2.21	20.22	5.65	0.31	13.02	7.83	832	○
	211.27	25.88	35.46	1.87	2.14	6.30	2.72	24.50	5.59	0.34	13.52		1008	○
	221.25	26.43	40.05	2.13	2.39	7.18	3.20	27.52	5.67	0.24	13.81		1132	○
Rough walls														
R1	232.40	28.51	14.90	0.86	0.87	2.82	1.33	–	6.69	0.19	12.88		773	△
	236.84	28.78	19.93	1.15	1.17	3.83	1.82	–	6.70	0.18	13.64		1041	△
	239.38	28.70	25.20	1.46	1.48	4.82	2.32	–	6.67	0.19	14.23	13.52	1310	△
	243.78	28.84	29.58	1.71	1.73	5.68	2.77	–	6.69	0.18	14.65		1539	△
	254.33	29.52	35.21	2.04	2.05	6.87	3.42	–	6.69	0.15	15.08		1821	△
R2	241.11	29.41	15.10	0.89	0.89	2.96	1.44	–	7.01	0.19	13.44		963	◇
	229.33	28.56	19.74	1.18	1.15	3.75	1.79	–	7.09	0.18	14.14	16.17	1263	◇
	229.34	28.25	24.90	1.49	1.46	4.68	2.27	–	7.12	0.18	14.74		1599	◇
	230.03	28.64	29.83	1.78	1.75	5.69	2.73	–	7.13	0.16	15.21		1920	◇
Porous-rough walls														
PR1	225.41	26.90	17.28	1.06	1.01	3.08	1.58	13.32	7.48	0.18	14.08		1235	☆
	218.12	27.17	21.47	1.31	1.26	3.90	1.92	16.74	7.49	0.15	14.66		1552	☆
	227.93	27.28	26.04	1.60	1.54	4.78	2.46	20.55	7.60	0.14	15.19	17.65	1906	☆
	226.64	27.33	31.49	1.94	1.85	5.74	2.94	24.65	7.60	0.09	15.65		2286	☆
	229.11	27.28	35.01	2.17	2.05	6.36	3.31	27.46	7.67	0.10	15.93		2547	☆
PR2	219.42	27.29	15.06	0.95	0.90	2.79	1.41	12.27	7.94	0.13	14.23		1254	☆
	221.73	27.41	19.97	1.26	1.20	3.75	1.91	16.40	7.93	0.13	14.98	19.45	1677	☆
	224.41	27.61	25.20	1.59	1.52	4.77	2.45	20.76	7.98	0.13	15.58		2122	☆
	222.96	28.06	28.26	1.79	1.69	5.40	2.71	23.16	8.00	0.14	15.86		2368	☆

Table 1: Summary of all test surfaces: baseline smooth walls (**S**), porous (**P**), rough (**R1** and **R2**), and porous-rough (**PR1** and **PR2**) walls. The statistics are obtained from HWA measurements: δ is the 99% boundary-layer thickness and θ is the momentum thickness.

Reynolds number definitions are: $Re_x \equiv xU_\infty/\nu$, $Re_\theta \equiv \theta U_\infty/\nu$, $Re_\tau \equiv \delta U_\tau/\nu$, and $Re_K \equiv \sqrt{K}U_\tau/\nu$. Coefficient of friction is defined as $C_f \equiv 2(U_\tau/U_\infty)^2$. The last column shows the symbol associated with each test surface. Colours denote test cases with approximately matched Re_τ and $Re_K \approx 14400$ and 13 (○), 18600 and 17 (○), 23400 and 20.5 (○), 27700 and 24 (○), 33100 and 27.5 (○).

with matched Re_τ and Re_K (within $Re_K \pm 10\%$), which runs from lighter towards darker colour as Re_τ and Re_K increases.

The porous walls are constructed from sheets of 15 mm-thick ($1060 \leq k^+ \equiv kU_\tau/\nu \leq 2130$), 45 ppi (pores per inch) polyurethane reticulated foam. The substrate has the average pore size of $s = 0.89$ mm ($63 \leq s^+ \equiv sU_\tau/\nu \leq 126$) and permeability of $K = 3.62 \times 10^{-8}$ m², corresponding to $13 \leq Re_K \leq 27.5$. The rough walls are constructed from two types of diamond-shaped, expanded metal mesh sheets denoted by **R1** and **R2** (figure 2b,c). The mesh sheets have the thickness of $k = 3$ and 3.5 mm ($178 \leq k^+ \leq 476$) for **R1** and **R2**, respectively, and the open area A_o (ratio of empty to total area in xz -plane) of 0.73 and 0.81. Both mesh sheets only cover a 1 m-wide portion (in z) of the working section (figure 2(a)(d)).

Details of the relevant parameters regarding the porous substrate and mesh geometries are given in figure 2(d).

2.3. Hot-wire anemometry

Hot-wire anemometry (HWA) measurements are conducted for all test surfaces listed in table 1 by traversing the wire in wall-normal direction y across 35–40 logarithmically-spaced points from the wall towards the freestream. All measurements are conducted at the centreline of the tunnel at $x = 8.8$ m from the datum of the tunnel test section (figure 2(a)(f)). A modified Dantec 55P05 single-sensor with a boundary-layer type probe (and an appropriate probe support) are used with a Streamline Pro Constant Temperature Anemometer (CTA) with an overheat ratio of 0.8. The sensor is a $5 \mu\text{m}$ diameter, 1-mm long tungsten wire soldered to the tip of the hot-wire prong, satisfying the recommended wire length-to-diameter ratio of 200 (Ligrani & Bradshaw 1987) and corresponding to the viscous-scaled sensor lengths of $57 \leq l_w^+ \equiv l_w U_\tau / \nu \leq 145$. The output signal is sampled from the CTA at $f_s = 30$ kHz, yielding viscous-scaled sampling interval of $1.6 \leq t^+ \equiv U_\tau^2 / (f_s \nu) \leq 10$. The sampling time T_s at each measurement point differs between test surfaces such that the boundary-layer turnover time is maintained at $T_s U_\infty / \delta \geq 20000$ to allow convergence of turbulence energy spectra (Hutchins *et al.* 2009). The sensor is traversed to the freestream and calibrated prior to and after each measurement. The relation between freestream velocity U_∞ and output voltage of the sensor E_∞ is defined by King’s law $E_\infty^2 = C_1 + C_2 U_\infty^3$. Temperature compensation is applied to the output signal to account for a slight sensor drift.

2.4. Wall shear stress (WSS) measurements

The WSSs of all test surfaces shown in table 1 are measured using an in-house floating element (FE) drag balance. The balance has a $200 \text{ mm} \times 200 \text{ mm}$ FE located at $x = 8.6$ m (figure 2(a)(e)), slightly upstream of the HWA measurement station. A section of each test surfaces are cut according to the size of the FE and mounted on top of the FE, leaving a 0.5 mm clearance between the FE and its housing, allowing it to move freely for WSS measurements. The housing is sealed to prevent airflow into the balance. Measurements are acquired at $f_s = 256$ Hz with 120 s sampling time for each test surface. Calibration of the balance is performed before measurements by loading a set of calibration weights to the balance via a pulley system. The relationship between known calibration weights and time-averaged output voltage (within $\pm 0.96\%$ uncertainties) from the balance is obtained by fitting the calibration data into a first order polynomial.

Figure 3(a) shows the C_f of all tests surfaces as a function of fetch Reynolds number $Re_x \equiv x U_\infty / \nu$. For validation, C_f of smooth walls ($2930 \leq Re_\tau \leq 12500$) are determined first using three different methods: (i) direct WSS measurements using the FE drag balance (\square), (ii) fitting velocity profiles obtained from HWA measurements to the composite profile of Rodríguez-López *et al.* (2015) (\blacksquare), (iii) the analytical solution of Monty *et al.* (2016) (—). All three methods show a reasonable agreement with each other to within 5%.

For the rest of the test surfaces **P**, **R**, and **PR**, C_f are determined from direct WSS measurements. Both rough walls (**R1** and **R2**) have higher C_f than that of porous walls, which increase further as the walls are combined with the porous walls (**PR1** and **PR2**), as shown in figure 3(a). The logarithmic shift ΔU^+ and k_s for these surfaces are obtained by fitting the mean profile to a modified method of Rodríguez-López *et al.* (2015), in which the log-law shift term ΔU^+ is added, forming equation (1.1) while maintaining the U_τ obtained from direct WSS measurements. The fit yields $\kappa = 0.39$ and $B = 4.34 \pm 0.08$ (consistent with those obtained for TBLs developing over various porous walls measured by Esteban *et al.* 2022). Porous wall C_f (figure 3a) is compared to the analytical solution proposed by Monty

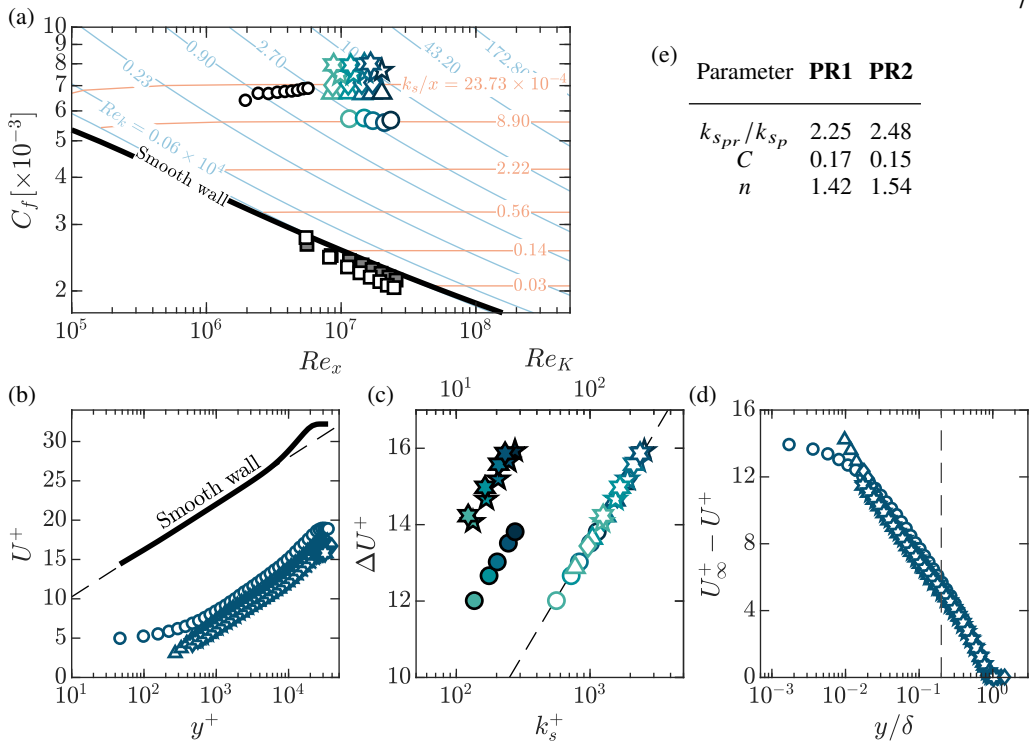


Figure 3: (a) C_f as a function of Re_x for all test surfaces. Validation of the WSS measurements with smooth walls (\square): fitted to the composite profile of Rodríguez-López *et al.* (2015) (\blacksquare) and the analytical solution of Monty *et al.* (2016) (\blacksquare). The same porous surface measured by Esteban *et al.* (2022) (\circ). Porous wall ($k_s = 7.83$ mm) at constant $Re_k \equiv kU_\infty/\nu$ (---) and constant k_s/x (---), obtained from Monty *et al.* (2016). (b) U^+ as a function of y^+ for matched $Re_\tau \approx 27700$, --- : $1/\kappa \ln y^+ + B$. (c) ΔU^+ as functions of k_s^+ (white-filled symbols, bottom axis) and Re_K (filled symbols, top axis). --- : $1/\kappa \ln k_s^+ + B - B_{FR}$. Legends are shown in table 1. (d) Velocity defect $U_\infty^+ - U^+$ as a function of y/δ for matched $Re_\tau \approx 27700$. (e) Decoupling of permeability and roughness effect using methods described in §3.

et al. (2016) over constant $k_s/x = 8.9 \times 10^{-4}$ ($k_s = 7.83$ mm). Additionally, C_f obtained by Esteban *et al.* (2022) for the same porous wall, $k_s/x = 2.4 \times 10^{-3}$ ($k_s = 7.97$ mm) is also compared with the analytical solution, both showing good agreement with these solutions.

Figure 3(b) shows the vertical downward shift in the logarithmic region for all test surfaces at a matched $Re_\tau \approx 27700$ (the highest matched Re_τ for **PR2** set and second highest for **PR1**) from a smooth wall TBL at this matched Re_τ . This shift, denoted by ΔU^+ , is shown as a function of k_s^+ in figure 3(c) for all test surfaces (white-filled contours). All collapse to the logarithmic function $1/\kappa \ln k_s^+ + B - B_{FR}$ (equation 1.2), although this is given since k_s is not obtained independently from ΔU^+ . The magnitude of k_s^+ (table 1) exceeds the threshold defined by Flack & Schultz (2010), $k_s^+ \gtrsim 70$, ensuring that all test surfaces are ‘fully’ rough and thus ΔU^+ depends solely on k_s . It should be noted that ΔU^+ here accounts for the total momentum deficit (from that of smooth wall TBLs) in both porous and rough walls, and it shows that it is possible to characterise porous wall with the same framework used for rough wall characterisation (i.e. logarithmic shift that scales on k_s). The effect of permeability on ΔU^+ is shown in figure 3(c) for test surfaces comprises of porous walls (**P**, **PR1**, and **PR2**, filled contours). Although it is clear that ΔU^+ is logarithmically scaled by Re_K , universality, as shown in figure 3(c) with k_s , is not apparent. This highlights the importance of accounting

for the ‘blockage’ effect (equation 1.5). At high range of Re_τ tested in this study, the outer layer similarity is preserved for all test surfaces (i.e. velocity defect profiles collapse beyond $y/\delta \gtrsim 0.2$, figure 3d), ensuring that a given value of k_s (for a surface) can be used to predict the drag at higher Reynolds numbers.

3. Decoupling permeability and roughness effect

3.1. Additional blockage effect

We rewrite equation (1.6) for porous wall (case **P**) in a more general term

$$k_{s_p} = Re_K f(k_{s_b}) \quad (3.1)$$

where $f(k_{s_b})$ is a function representing the blockage effect by the substrate. As a roughness interface is added (case **PR**), a roughness term, possibly a function of the characteristic lengthscale of roughness (i.e. rough wall k_s) increases blockage

$$k_{s_{pr}} = Re_K f(k_{s_b}, k_{s_r}) \quad (3.2)$$

where subscripts ‘r’ denotes the rough wall and ‘pr’ the porous-rough wall. When two substrates have an approximately matched permeability, then the additional blockage effect can be approximated by $f(k_{s_b}, k_{s_r})/f(k_{s_b}) \approx k_{s_{pr}}/k_{s_p}$. Case **PR1** has 5 matched Re_K with case **P** (within 5% difference, table 1). As the k_s for these surfaces are known from fitting ΔU^+ (§2.4), the additional blockage is approximated by $f(k_{s_b}, k_{s_r})/f(k_{s_b}) = 2.25$ (figure 3e) within 10% error due to Re_K difference. This is interpreted as the rough wall **R1** increases the total blockage effect by approximately 2.25 times from that of porous wall.

At this point, the empirical formulation of $f(k_{s_b}, k_{s_r})$ is unknown. Let the roughness effect be represented solely by rough wall k_s

$$f(k_{s_b}, k_{s_r}) = f(k_{s_b}) C k_{s_r} \quad (3.3)$$

where C is a constant. For an approximately matched Re_K , $C \approx k_{s_{pr}}/(k_{s_p} k_{s_r})$. We obtain $C = 0.17$ for case **PR1** (figure 3e), and further test this formulation for the second roughness **PR2**. Here, there are 4 matched Re_K cases (within 10% difference, table 1). The total blockage effect increases by approximately 2.5 times from the porous wall (figure 3e), consistent with the increasing C_f of case **R2** from that of **R1** (figure 3a). The constant C appears to be similar to that obtained from **R1**, $C = 0.15$. This suggest that the formulation has the potential to be applicable across different cases and is not dependent on the type of roughness.

3.2. Equivalent homogeneous roughness

A recent study by Hutchins *et al.* (2023) suggested that for a heterogeneous rough wall (i.e. a rough wall constructed from various patches of homogeneous roughness of roughness length scale k_{s_i} covering an area A_i), the equivalent homogeneous roughness length k_{ehr} can be defined as:

$$k_{ehr} = \left[\frac{1}{A} \sum_{i=1}^N k_{s_i}^n A_i \right]^{\frac{1}{n}} \quad \text{where} \quad A = \sum_{i=1}^N A_i \quad (3.4)$$

In the present study, the drag penalty from all test surfaces can be represented by the logarithmic shift ΔU^+ (figure 3b), suggesting the possibility of characterising permeable walls with the same framework used for rough wall TBLs. Thus, we might consider porous-rough walls as simply a combination of two ‘homogeneous roughnesses’ overlaying each

other. Equation (3.4) is therefore reduced to

$$k_{s_{pr}} = \left[k_{s_p}^n + k_{s_r}^n \right]^{\frac{1}{n}} \quad (3.5)$$

For case **PR1**, n is obtained by solving equation (3.5) with the known k_s for each **PR1**, **P**, and **R1**, resulting in $n = 1.42$. The same approach is applied to case **PR2**, resulting in $n = 1.54$, which is relatively consistent with that obtained from case **PR1**.

It is still unknown, at this point, what the empirical formulation for the roughness effect is. Present results suggest that it is possibly in terms of an additional logarithmic shift similar to equation (1.5). Further, it is still unclear what the empirical relation with the characteristic lengthscale of roughness (rough wall k_s) is. For the two methods tested in §3, it is neither understood what the physical interpretations of constants C and n are, nor whether these constants are universal for various types of rough walls. We are unable to answer these questions in this study. However, present results suggest a promising start towards decoupling permeability and roughness effects.

4. Conclusions and future work

We conduct velocity and drag measurements of TBLs developing over various porous-rough wall combinations, with the roughness effect systematically varied while maintaining the permeability effect. Measurements are conducted at relatively high Reynolds numbers ($14400 \leq Re_\tau \leq 33100$), with a set of matched Re_τ (within 10%) and Re_K ($13 \leq Re_K \leq 27.5$) of each porous-rough combinations. Present results suggest that the increase in drag over porous, rough, and porous-rough walls is characterised by a downward shift in the logarithmic region ΔU^+ from that of smooth wall TBLs and that the mean flow follows outer-layer similarity for cases examined at these high Reynolds numbers (with substantial scale separation). Further analysis shows that ΔU^+ from these surfaces can be characterised by the roughness lengthscale k_s , suggesting the possibility of characterising porous walls with the same framework used for rough wall TBLs. Following the hypothesis of Esteban *et al.* (2022), it is viable that for a porous-rough wall, permeability and roughness effects are represented by Re_K and a total blockage function $f(k_{s_b}, k_{s_r})$, respectively, with the total blockage consists of the blockage effect from the porous substrate and additional roughness interface above the porous wall. Present results suggest that the rough walls increase the blockage of porous-rough walls by approximately 2.3–2.5 times from that of the porous wall for both roughnesses tested in this study. We observed that the additional roughness effect follows Ck_{s_r} , where constant $C \approx 0.16$ for both rough wall test surfaces. Analysis of the same data with the method suggested by Hutchins *et al.* (2023) shows that the effect of porous and rough walls may be decoupled using an area-weighted power-mean (with $n \approx 1.5$ for both surfaces) to obtain an equivalent roughness length for both rough wall test surfaces. The empirical formulation as well as the physical interpretation of constants observed in this study requires further data and should be the focus of future work.

Funding. We gratefully acknowledge the financial support from EPSRC (Grant Ref no: EP/S013296/1) and European Office for Airforce Research and Development (Grant No: FA9550-19-1-7022, Programme Manager: Dr. Doug Smith).

Declaration of interest. The authors declare no conflict of interest.

Data availability statement. The data that support the findings of this study will be made available upon publication.

Author ORCID. D. D. Wangsawijaya: [0000-0002-7072-4245](https://orcid.org/0000-0002-7072-4245), P. Jaiswal: [0000-0002-5240-9911](https://orcid.org/0000-0002-5240-9911), B. Ganapathisubramani: [0000-0001-9817-0486](https://orcid.org/0000-0001-9817-0486)

Author contributions. PJ and DDW designed, carried out measurements, and post-processed the data. DDW analysed the data and wrote the manuscript, BG was responsible for conceptualisation, funding acquisition, editing of drafts and project management.

REFERENCES

- BREUGEM, W. P., BOERSMA, B. J. & UITTENBOGAARD, R. E. 2006 The influence of wall permeability on turbulent channel flow. *J. Fluid Mech.* **562**, 35–72.
- EFSATHIOU, CHRISTOPH & LUHAR, MITUL 2018 Mean turbulence statistics in boundary layers over high-porosity foams. *J. Fluid Mech.* **841**, 351–379.
- ESTEBAN, L. B., RODRÍGUEZ-LÓPEZ, E., FERREIRA, M. A. & GANAPATHISUBRAMANI, B. 2022 Mean flow of turbulent boundary layers over porous substrates. *Phys. Rev. Fluids* **7** (9), 094603.
- FLACK, K. A. & SCHULTZ, M. P. 2010 Review of hydraulic roughness scales in the fully rough regime. *J. Fluids Eng.* **132** (4), 041203.
- HAHN, SEONGHYEON, JE, JONGDOO & CHOI, HAECHON 2002 Direct numerical simulation of turbulent channel flow with permeable walls. *J. Fluid Mech.* **450**, 259–285.
- HAMA, F. R. 1954 Boundary-layer characteristics for rough and smooth surfaces. *Trans. SNAME* **62**, 333–351.
- HUTCHINS, N., GANAPATHISUBRAMANI, B., SCHULTZ, M. P. & PULLIN, D. I. 2023 Defining an equivalent homogeneous roughness length for turbulent boundary layers developing over patchy or heterogeneous surface. *Ocean Eng.* **271**, 113454.
- HUTCHINS, N., NICKELS, T. B., MARUSIC, I. & CHONG, M. S. 2009 Hot-wire spatial resolution issues in wall-bounded turbulence. *J. Fluid Mech.* **635**, 103–136.
- KONG, F. & SCHETZ, J. 1982 Turbulent boundary layer over porous surfaces with different surface geometries. *In the 20th AIAA Aerospace Sciences Meeting.*
- LIGRANI, P. M. & BRADSHAW, P. 1987 Subminiature hot-wire sensors: development and use. *J. Phys. E: Sci. Instrum.* **20**, 323–332.
- MANES, C., POGGI, D. & RIDOLFI, L. 2011 Turbulent boundary layers over permeable walls: scaling and near-wall structure. *J. Fluid Mech.* **687**, 141–170.
- MANES, COSTANTINO, POKRAJAC, DUBRAVKA, MCEWAN, IAN & NIKORA, VLADIMIR 2009 Turbulence structure of open channel flows over permeable and impermeable beds: A comparative study. *Phys. Fluids* **21**, 125109.
- MONTY, J. P., DOGAN, E., HANSON, R., SCARDINO, A. J., GANAPATHISUBRAMANI, B. & HUTCHINS, N. 2016 An assessment of the ship drag penalty arising from light calcareous tubeworm fouling. *Biofouling* **32** (4), 451–464.
- NIKURADSE, J. 1933 Strömungsgesetze in rauhen rohren. *VDI Forschungsheft* **361**, English translation: 1950 Laws of flow in rough pipes. *NACA Tech. Mem.* **1292**.
- RODRÍGUEZ-LÓPEZ, E., BRUCE, P. J. K. & BUXTON, O. R. H. 2015 A robust post-processing method to determine skin friction in turbulent boundary layers from the velocity profile. *Exp. Fluids* **56**, 68.
- ROSTI, MARCO E., CORTELEZZI, LUCA & QUADRIO, MAURIZIO 2015 Direct numerical simulation of turbulent channel flow over porous walls. *J. Fluid Mech.* **784**, 396–442.
- SHIMIZU, Y., TSUJIMOTO, T. & NAKAGAWA, H. 1990 Experiment and macroscopic modelling of flow in highly permeable porous medium under free-surface flow. *J. Hydrosoci. Hydraul. Eng.* **8** (1), 69–78.
- SUGA, K., MATSUMURA, Y., ASHITAKA, Y., TOMINAGA, S. & KANEDA, M. 2010 Effects of wall permeability on turbulence. *Int. J. Heat Fluid Flow* **31**, 974–984.
- ZAGNI, ANTHONY F. E. & SMITH, KENNETH V. H. 1976 Channel flow over permeable beds of graded spheres. *J. Hydraul. Div.* **102** (2), 207–222.
- ZIPPE, HANS J. & GRAF, WALTER H. 1983 Turbulent boundary-layer flow over permeable and non-permeable rough surfaces. *J. Hydraul. Res.* **21** (1), 51–65.